THE JOURNAL OF Ammonia Energy

Available online at

jae.cardiffuniversitypress.org

ISSN **2752-7735**
The Journal of Ammonia Energy 02 (2024) 073–084

Cardiff University Press | Gwasg Prifysgol Caerdydd

A numerical study of ammonia combustion in spark-ignition and reactive-fuel pilot-ignition engines

Sforza L[a*], Ballerini A[a], Ramognino F[a], Schirru A[a], Lucchini T[a], D'Errico G[a], Dupuy A[b], Rabello de Castro R[b] , Brequigny P[b] , Mounaïm-Rousselle C[b]

[a]*Politecnico di Milano, Department of Energy, via Lambruschini 4a, 20156, Milan, Italy*
[b]*Université Orléans, INSA-CVL, PRISME, EA 4229, F45072, Orléans, France*

Abstract

Decarbonizing internal combustion engines (ICEs) requires the use of fuels produced from renewable energy, with easy storage and characterized by a combustion process with zero carbon dioxide (CO_2) emissions. Ammonia (NH_3) perfectly fits all these requirements. However, its use as fuel for ICEs calls into question many of the consolidated aspects related to ignition and flame propagation processes studied during the last decades. NH_3 differs from conventional hydrocarbon fuels for a higher minimum ignition energy and auto-ignition temperature, as well as for a lower combustion speed and energy density. Experimental investigations carried out in both metal and optical engines proved the feasibility of NH_3 operation as pure fuel in spark-ignition (SI) engines or in reactive-fuel pilot-ignition (RFPI) engines with a pilot injection of a high-reactivity fuel. In this work, computational fluid dynamics (CFD) methodologies consolidated with conventional fuels are applied to simulate a selection of operating points on such experiments. The flame area model (FAM) from Weller is employed for the SI operation, while the tabulated well-mixed (TWM) model is used for the RFPI mode. The effects from a NH_3-air dilution, a spark-timing advance and an increase in injection duration are studied to identify the main challenges related to the NH_3 combustion modelling in ICEs. The results show that numerical models capture the measured trend of spark-timing and injection duration variations at both stoichiometric and lean NH_3-air mixtures. However, for the SI mode, aspects such as the laminar-to-turbulent transition stage and the heat release rate dependency on the ignition time require further modeling improvements. Similarly, for the RFPI mode, the auto-ignition delay of the dual-fuel mixture and the turbulent flame speed are numerically underestimated. Therefore, all these aspects represent challenges that need to be addressed in CFD models to improve NH_3 ignition and combustion prediction.

Received: 22nd Jan 24; Accepted: 11th Jun 24; Published: 4th Jul 24

Keywords: Ammonia premixed combustion, spark-ignition engines, reactive-fuel pilot-ignition engines, computational fluid-dynamics, flame area model, tabulated well-mixed model.

Introduction

The ongoing energy transition process towards renewable and zero-carbon emissions sources demands a rapid evolution of the internal combustion engine (ICE) technology, which has been optimized for fossil fuels usage during the last decades. Considering that chemical energy storage represents the most flexible and robust mechanism to store energy [1], ICEs are expected to be crucial for both power generation and hard-to-abate transportation sectors, like trucks and ships.

In this context, ammonia (NH_3) represents an ideal candidate as fuel for ICEs. It is carbon-free, it can be easily stored and delivered as liquid at ambient temperature and low pressure (8 bar) in an existing infrastructure, and its production process can be entirely based on renewable power sources [2].

Several experimental studies demonstrated the feasibility of NH_3 operation in ICEs. Lhuillier et al. [3] tested pure NH_3-air premixed combustion in a retrofitted spark-ignition (SI) gasoline engine with a moderate compression ratio (10.5), observing low cyclic variability and power outputs like those obtain with methane (CH_4), if near-stoichiometric lean operations are selected. Therefore, despite the low laminar burning velocity, pure ammonia combustion is assumedly mainly driven by the ignition kinetics and the flame response to turbulence. Jespersen et al. [4] investigated the effects of spark energy and discharge characteristics on the lean-burn characteristics of NH_3 in a premixed SI research engine, observing how combustion stability is sensitive to ignition system choice and spark timing. To promote ammonia ignition and combustion, several strategies have been tested. A multiple spark-plug approach was

* Corresponding author. E-mail address: lorenzo.sforza@polimi.it
https://doi.org/10.18573/jae.29

studied by Uddeen et al. [5], resulting in a reduced combustion duration and higher engine power output. The spark-assisted compression ignition (SACI) mode was explored by Mounaïm-Rousselle et al. [6] and Reggeti et al. [7], where the premixed NH_3-air charge is first ignited by a spark, then auto-ignition is promoted in the end-gas by flame expansion and high compression ratios (up to 18). The observed burn process was significantly faster than a traditional turbulent flame propagation, which allowed to extend the engine operating range, especially at low loads.

The addition of hydrogen (H_2) as combustion promoter was also tested [8], showing that H_2 enrichment enhances the NH_3 combustion efficiency and helps reducing its exhaust concentration. However, optimal H_2 enrichments around 10-20% by volume are required [9, 10], hence a significant H_2 quantity needs to be supplied by a storage tank or reformed onboard from ammonia [11, 12].

A promising technique to enhance the ignition kinetics of NH_3 engines demonstrated to be the reactive-fuel pilot-ignition (RFPI) mode. This strategy exploits the high NH_3 auto-ignition temperature and consists in a compression-ignition of a small quantity of a high-reactivity liquid fuel, injected into a NH_3-air charge. This method is extremely favorable for the abatement of carbon-based emissions from large-bore maritime engines applications, where a significant ignition energy is required [13]. Dupuy et al. [14] investigated the RFPI operation on a single-cylinder metal engine over a wide range of NH_3-air equivalence ratios, testing different durations and energy fractions of a diesel pilot injection. They demonstrated that minimizing the diesel amount of the pilot injection does not guarantee the minimal carbon footprint, while a combined optimization between the diesel energy fraction and the premixed NH_3-air equivalence ratio is required.

Other experimental studies on ammonia RFPI-like operation with diesel injection are available in the literature, attempting to clarify combustion and emission characteristics. Hiraoka et al. [15] observed an elongation of the NH_3-diesel ignition delay if the ammonia energy fraction is increased. Imamori et al. [16] compared the diesel-ammonia RFPI mode with the conventional diesel combustion, showing that increasing the NH_3 energy fraction to 94% leads to a reduction of the greenhouse gas emissions by 82%. The effect of the diesel injection parameters was investigated by Liu et al. [17], who clarified how an increase of both injection pressure and timing enhanced the chemical reactivity of in-cylinder mixture, leading to a shorter ignition delay. Instead, Mounaïm-Rousselle et al. [18] and Mi et al. [19] studied the effect of splitting the diesel injection into two parts, a pilot and a main one. This strategy proved benefits in terms of diesel-ammonia-air mixture reactivity, with a reduction of nitrogen oxides (NO_x), carbon monoxide (CO) and unburned NH_3 emissions. Zhang et al. [20] investigated the compression-ignition of ammonia by an injection of n-heptane in an optical, pent-roof, single-cylinder engine, in which tumble or combined swirl-tumble flows were tested. The optimization of fuel injection and flow arrangement demonstrated to yield high-efficient combustion process, maintaining NO_x and NH_3 emissions within reasonable levels.

However, to enhance the understating of ignition kinetics, combustion evolution and emissions formation, computational fluid dynamics (CFD) analyses are needed to support the experimental activity available in the literature. Reliable CFD models and methodologies are crucial to properly describe the complex phenomena occurring in ammonia ICEs. Nevertheless, NH_3 is characterized by different thermochemical properties with respect to conventional hydrocarbon fuels, such as: higher minimum ignition energy and auto-ignition temperature; lower combustion speed and energy density. Consequently, many consolidated aspects related to ignition and flame propagation processes, studied during last decades on hydrocarbon fuels, need to be assessed if ammonia is used.

In this work, CFD approaches extensively used in the past to study combustion of conventional fuels [21–24] are here employed to simulate, on the same metal engine, the NH_3 operation in both SI and RFPI modes. A conventional ignition system with a single spark-plug and diesel as high-reactivity fuel are employed, respectively. The flame area model (FAM) is chosen for the SI operation, while the tabulated well-mixed (TWM) model is used for the RFPI mode. Despite this work represents only the first step of a large-scale study, some critical aspects related to NH_3 combustion modelling in ICEs are identified by investigating the effects from a NH_3-air equivalence ratio reduction, a spark-timing advance and an increase of injection duration. Therefore, specific challenges for current CFD approaches are pointed out and some improvements are also proposed. However, all these numerical deficiencies are urged to be addressed to achieve a more reliable modelling of NH_3 combustion inside ICEs.

Experimental configuration

A DW10 four-cylinder light-duty engine, converted into a 0.5 l single-cylinder, is selected as experimental reference for the present study. Table 1 reports its main geometrical features, while all

details of the experimental setup are shown in Fig. 1. All times are here reported in crank-angle degrees (°CA) after top dead center (aTDC) at which the combustion event occurs. The engine, characterized by a flat-head and a re-entrant piston bowl shape, can be operated alternatively with both SI and RFPI modes by replacing the central spark-plug with a direct injector (DI). Diesel is selected as high-reactivity fuel for the RFPI operation.

Experimental tests are conducted at a constant engine speed of 1000 rpm, measuring different NH_3-air equivalence ratios ϕ and ignition timings, in terms of spark-advance (SA) for the SI mode or duration of injection (DOI) for the RFPI mode. The start of injection (SOI) of diesel fuel is kept constant at -11 °CA. The measured operating conditions studied in this work are reported in Tables 2 and 3, respectively. The indicated mean effective pressure (IMEP) values are included as well. The amounts of diesel energy share E_{diesel} of the total energy available inside the cylinder (NH_3 + diesel) are also reported for each RFPI case in Table 3. As it can be observed, the small quantities of injected high-reactivity fuel confirm the main feature of the RFPI operation, namely a premixed combustion of NH_3 and air which is triggered by the autoignition of a small diesel-NH_3-air mixture. This differs from typical dual-fueling modes, where the non-premixed fuel can have a significant percentage of the total closed-valve energy share.

Table 1. Single-cylinder engine features.

Feature	Value
Bore x Stroke (mm x mm)	85 x 88
Conn. Rod length (mm)	141
Engine speed (rpm)	1000
Intake valve opening/closing	-117/344 °CA
Exhaust valve opening/closing	134/396 °CA
Swirl ratio (50 CAD BTDC)	2.0
Compression ratio (-)	16.42
Ignition type	SI or RFPI
Main fuel	NH_3
High-reactivity fuel	Diesel

A Kistler 6045A relative quartz pressure transducer, integrated with a LabView data acquisition system, is employed to acquire the in-cylinder pressure with a resolution of 0.1 CAD. The temperature and pressure at both intake and exhaust manifolds are acquired by K thermocouples and resistive absolute pressure transducers, respectively. Ammonia fuel is stored in a tank as liquid and heated to be mixed in gas form with air. Brooks thermal flowmeters are employed to measure both NH_3 and air flow rates.

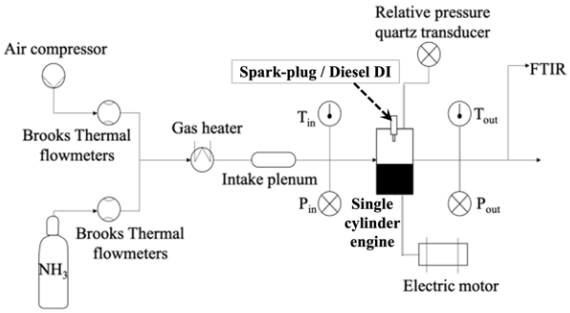

Fig. 1. Schematic of the experimental rig

For the SI operation, the same spark-plug used in [3] is adopted, with a coil charging time set to 2 ms. A Bosch 7-hole common rail injector (CRI) is employed for the RFPI operation keeping the diesel injection pressure P_{inj} at 200 bar to ensure flexibility on the injection duration. For each operating condition, the average-cycle pressure trace is calculated from the record of 200 consecutives cycles of pressure data. For more details about the heat release rate calculation and the exhaust gases analysis, the reader is referred to [14, 3].

Table 2. SI mode: measured operating conditions.

Condition	IMEP [bar]	ϕ [-]	SA [°CA]
ER0.85-SA-24	6	0.85	-24
ER0.85-SA-35	6	0.85	-35
ER1.00-SA-18	7	1	-18
ER1.00-SA-25	7	1	-25

Table 3. RFPI mode: measured operating conditions.

Condition	IMEP [bar]	ϕ [-]	DOI [μs]	SOI [°CA]	E_{diesel} [%]
ER0.85-DOI450	7	0.85	450	-11	2.3
ER0.85-DOI550	7	0.85	550	-11	4.6
ER1.00-DOI450	7.5	1	450	-11	2.0
ER1.00-DOI550	7.5	1	550	-11	4.1

Numerical models

3D-CFD numerical simulations are carried out with Lib-ICE, a software based on the OpenFOAM® technology and developed by the authors to simulate

gas-exchange and reacting processes inside ICEs [25–28]. Transport equations are solved with the Reynolds Averaged Navier-Stokes (RANS) approach, where turbulence is described with the standard $k-\varepsilon$ model.

SI combustion

The numerical approach selected to model the SI premixed combustion of the NH_3-air mixture is shown by Fig. 2. The flame area evolution (FAE) model is employed for the reaction rate prediction, considering its success in simulating both CH_4 and H_2 premixed combustion [29–31]. The flame front propagation is modelled according to the following transport equation [32],

$$\frac{\partial \rho \tilde{b}}{\partial t} + \nabla \cdot \left(\rho \tilde{\boldsymbol{U}} \tilde{b}\right) + \nabla \cdot \left(\mu_t \nabla \tilde{b}\right) = \rho_u \widetilde{S_u} \tilde{\Xi} |\nabla \tilde{b}| + \dot{\omega}_{ign} \tag{1}$$

where b is the unburned mass fraction (or regress variable), ρ and ρ_u the mixture and unburned mixture densities, $\boldsymbol{U}$ the mean flow velocity vector, S_u the laminar flame speed and μ_t the turbulent dynamic viscosity.

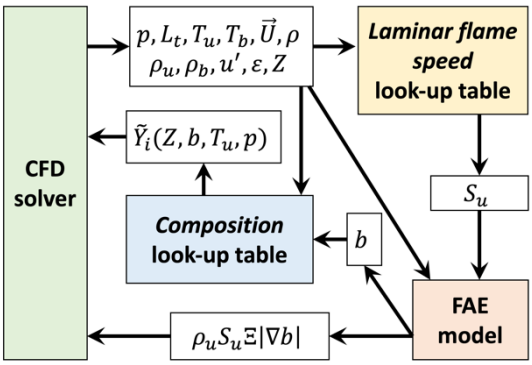

Fig. 2. Numerical model for combustion prediction with SI mode

A simplified deposition model is employed to mimic the ignition through the source term $\dot{\omega}_{ign}$ [26], while the flame wrinkle factor Ξ includes the flame-turbulence interaction effect by means of the turbulent to laminar flame speed ratio (S_t/S_u). This phenomenon is modelled according to a one-equation approach [32],

$$\Xi = f\,\Xi_{eq} = f\left\{1 - \frac{a_4 b_3^2}{2b_1}\frac{L_t}{\delta_l} + \left[\left(\frac{a_4 b_3^2}{2b_1}\frac{L_t}{\delta_l}\right)^2 + a_4 b_3^2 \frac{u'}{S_u}\frac{L_t}{\delta_l}\right]^{\frac{1}{2}}\right\} \tag{2}$$

where a uniform Ξ value is assumed across the flame brush. The laminar-to-turbulent transition process, taking place after the ignition event, is included through the f parameter according to [29, 33], which provides a smooth variation of Ξ from 1 (laminar flame) to its final equilibrium value Ξ_{eq} (fully turbulent flame). The equilibrium wrinkle factor Ξ_{eq} is modelled according to Peters [34], where δ_l is the laminar flame thickness, u' the turbulence intensity, while a_4, b_3 and b_1 are model constants.

The laminar flame speed S_u and the chemical composition are retrieved from lookup tables, generated in the OpenSMOKE framework [35] through a series of 1D and homogeneous reactor calculations, respectively, by using the Stagni mechanism [36]. These computations are performed at different constant pressure, unburned gas temperature and equivalence ratio conditions. The chemical composition of any computational cell is computed from the mass fraction of chemical species in the burned Y_b and unburned Y_u state, and from the regress variable b, where Y_b value is recovered at equilibrium conditions. The details for the lookup table generation are available in [37].

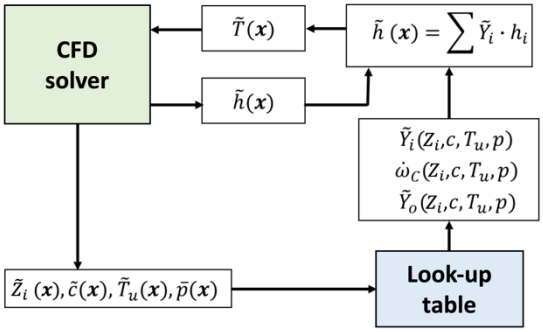

Fig. 3. The tabulated well-mixed (TWM) model for combustion prediction with RFPI mode

RFPI combustion

The tabulated well-mixed (TWM) approach is selected to model the RFPI combustion operation [37]. The model schematic is reported in Fig. 3. The mixture fraction equations for each fuel Z_i (here Z_{diesel} and Z_{NH_3}) are transported to consider the diesel-ammonia stratification,

$$\frac{\partial \rho \tilde{Z}_{diesel}}{\partial t} + \nabla \cdot \left(\rho \tilde{\boldsymbol{U}} \tilde{Z}_{diesel}\right) - \nabla \cdot \left(\mu_t \nabla \tilde{Z}_{diesel}\right) = \dot{S}_{Z_{diesel}}$$

$$\frac{\partial \rho \tilde{Z}_{NH_3}}{\partial t} + \nabla \cdot \left(\rho \tilde{\boldsymbol{U}} \tilde{Z}_{NH_3}\right) - \nabla \cdot \left(\mu_t \nabla \tilde{Z}_{NH_3}\right) = 0 \tag{3}$$

including the liquid diesel evaporation source term $\dot{S}_{Z_{diesel}}$. KH-RT model is used as diesel spray break-up model, while n-heptane is selected as

diesel surrogate. The progress variable, defined according to [38],

$$C = \sum_{i=1}^{N_s} h_{298,i}\, Y_i(t) - \sum_{i=1}^{N_s} h_{298,i}\, Y_i(0) \tag{4}$$

is used to track of the combustion evolution and it is transported inside the computational domain by means of,

$$\frac{\partial \rho \tilde{C}}{\partial t} + \nabla\left(\rho \tilde{\boldsymbol{U}} \tilde{C}\right) - \nabla\left(\frac{\tilde{\mu}_t}{Sc_t} \nabla \tilde{C}\right) = \rho \dot{C} \tag{5}$$

where Sc_t is the turbulent Schmidt number, while $\dot{C}$ is the progress variable source term. To correctly capture the auto-ignition of the diesel jet in the ammonia-air mixture, a lookup table is generated by means of homogeneous constant-pressure reactor calculations performed in the OpenSMOKE framework [35]. The CRECK C1-C16 high-temperature mechanism [39, 40] is selected to model the n-heptane-ammonia reaction kinetics.

To this end, four control variables are employed - unburned gas temperature, pressure and the mixture fraction of the two considered fuels. The lookup table is generated according to [37], where also the progress variable reaction rate $\dot{C}$ and the mixture composition Y_i are stored.

Numerical setup

The CFD simulations are carried out over the power-cycle only, from intake valve closing (IVC) to exhaust valve closing (EVC). Two different computational mesh grids are selected to study each ignition strategy (SI and RFPI) and their features are reported in Table 4. A 2D axisymmetric wedge domain is employed to model SI operation, thanks to the symmetrical properties of the flat cylinder head and the piston bowl. However, for the RFPI mode a 3D wedge domain representing 1/7 of the cylinder volume is used, because of the 7-hole diesel injector layout.

Table 4. 3D mesh features used for each analyzed ignition strategies (SI and RFPI). TDC = top dead center; BDC = bottom dead center.

Feature	SI mode	RFPI mode	U.o.M.
Wedge angle	1	51.43	[°]
TDC BDC	2.6	135.2	[k cells]
Average cell side	15	780	[k cells]
	0.35	0.35	[mm]

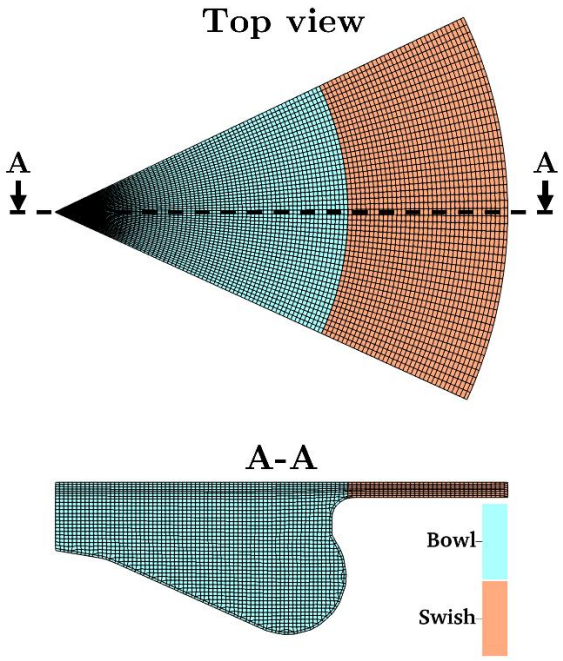

Fig. 4. Computational mesh features showed over a top view and an axial 2D cut plane at the TDC.

The SI and RFPI computational grids are characterized by similar internal features, as shown by Fig. 4, where the in-bowl and squish regions are also identified. A single boundary layer of 0.2 mm is used over all boundaries to ensure optimal operation of the wall functions ($y^+ > 30$), while a mesh refinement up to a 0.15 mm of cell side is applied in the squish area, to guarantee at least 8 cells along the axial direction. The dynamic addition/removal of layers is employed to mimic the piston displacement. This technique has been extensively used and validated in previous works [41-44].

A 3D swirl motion and a homogeneous mixture of ammonia and air are assumed, with initial conditions at IVC estimated by a 1D model of the entire engine layout, in which the measured heat release rate (HRR) and heat losses are imposed. The agreement of the 1D computed in-cylinder pressure and both air and ammonia mass flow rates are verified against measurements. The first is shown in Fig. 5 where, taken as example condition ER0.85-SA-35 (see Table 2), the dynamics of the engine breathing are rather well captured in SI mode. The second comparison is reported in Fig. 6, where the maximum 1D-experimental discrepancy is lower than 3%.

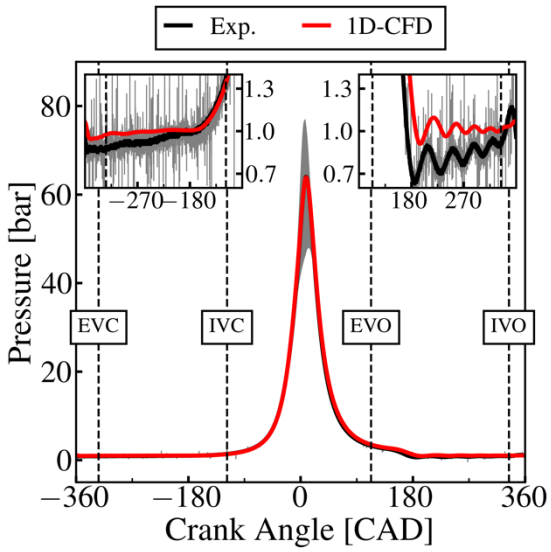

Fig. 5. Condition ER0.85-SA-35 (see Table 2). Numerical 1D-experimental comparison of the average-cycle in-cylinder pressure trace. The grey shaded area represents the variability of the 200 measured consecutive cycles.

In this preliminary 3D analysis, the exhaust gases presence is neglected at IVC, as the results from 1D engine simulations showed low EGR amounts (≤ 5%) for all conditions of Tables 2 and 3. Moreover, the estimated EGR value was consistent among all operating points, hence it is not expected to affect the main outcomes of this investigation.

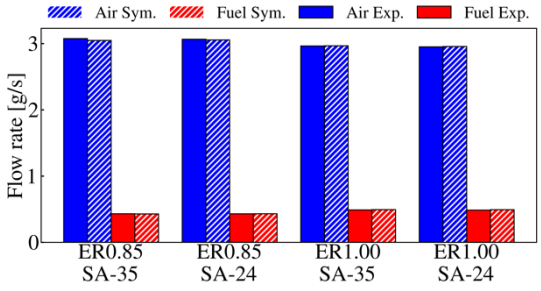

(a)

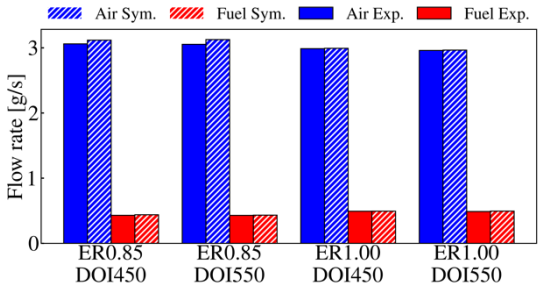

(b)

Fig. 6. Comparison between 1D simulations (Sym.) and measured values (Exp.) of air and NH_3 mass flow rates over the conditions of: (a) Table 2; (b) Table 3.

Finally, for RFPI cases, a simple triangular-shaped profile is imposed for the diesel injection process, ensuring that the total injected mass is consistent with the experimental value.

SI mode: results and discussion

3D-CFD simulations are carried out on the four operating conditions of Table 2. The computed results in terms of in-cylinder pressure and apparent heat release rate (AHRR) trends are reported in Fig. 7 and compared against experimental measurements of the engine average-cycle.

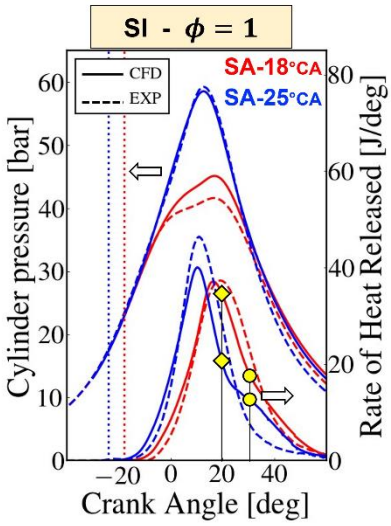

(a)

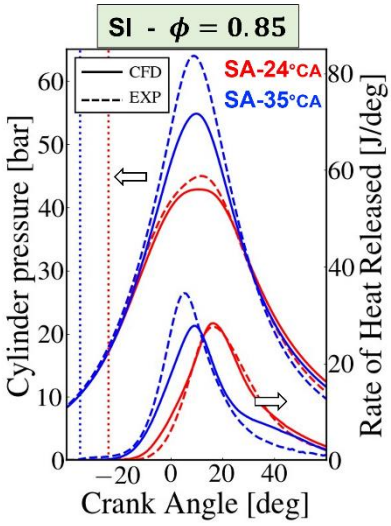

(b)

Fig. 7. SI mode: numerical-experimental comparison between pressure and apparent heat release rate (AHRR) evolutions inside the cylinder of the conditions in Table 2. The yellow squares and circles spot the AHRR values of instants analyzed in Fig. 8 top row and bottom row, respectively. The vertical dotted lines identify the spark-advance positions.

Focusing on the two cases operated at stoichiometric conditions (Fig. 7a), a satisfactory agreement is observed between computed results and measurements during the laminar-to-turbulent transition stage and the first part of the turbulent combustion development. The experimental trend produced by a spark-timing variation is properly captured by the simulations despite a slight underestimation of the transition stage duration. This can be probably caused by an electrical delay affecting the ignition system, which here is not considered in the numerical approach.

Moving to the completion stage of the turbulent combustion inside the piston bowl (Fig. 7a, at AHRR peak values and near after), it can be observed that numerical results are strongly influenced by a variation of the spark-timing if compared to measurements. In fact, advancing the ignition event from -18 °CA to -25 °CA, the computed energy release rate from combustion inside the bowl does not increase similarly to the observed experimental trend (almost perfect match for SA-18°CA condition, underestimation for SA-25°CA case). This probably produces a higher amount of unburned NH_3 forced into the squish region for the SA-25°CA case, where a higher AHRR is observed after 20 °CA if compared to the experimental trace.

The last combustion stage, which is characterized by the combustion inside the squish region, can be identified in Fig. 7a: 1) after the yellow square for the SA-25°CA case and 2) after the yellow circle for the SA-18°CA case. As is can be observed, such phase is affected by a light numerical overestimation of the AHRR for the SA-18°CA case and larger ones for the SA-25°CA case.

This discrepancy could be affected by multiple aspects. The previous discussed higher amount of unburned NH_3 in the squish region boosts the numerical overestimation of the SA-25°CA condition. Moreover, also the flame area extension during this stage could impact significantly, considering that typical low turbulence values are detected in the end-gas.

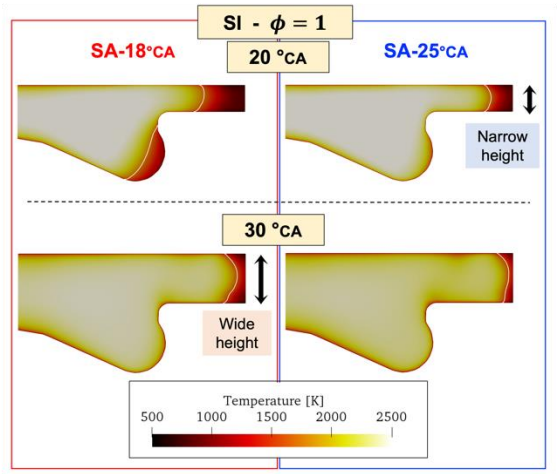

(a) **(b)**

Fig. 8. SI mode, ϕ = 1: computed temperature distribution for conditions of Fig. 7a at the highlighted time instants with yellow squares (20 °CA) and circles (30 °CA). The white line detects the flame front position (b = 0.5).

Figure 8 shows the flame front position of the SA-18°CA and SA-25°CA cases at 20 °CA and 30 °CA. These time instants are highlighted in Fig. 7a with yellow squares and circles, respectively. As it can be observed, when the ignition time is advanced, the flame front propagates inside the squish region with a narrow piston-head distance (Fig. 8b, top image). This produces a near annular flame area with a limited axial extension. Therefore, the energy is released slowly by the combustion process, until the flame hits the liner wall. On the contrary, with a delayed ignition time, the flame front is detected into the squish region when a wider distance is available between the piston and the cylinder head (Fig. 8a, bottom image). Consequently, a wider axial extension of the flame area is observed, with a consequent higher heat release rate and shorter combustion duration.

The adopted combustion model, instead, seems not to affect the numerical prediction of this final combustion stage, because the flamelet assumption (on which the FAE approach relies) is valid for both SA-18°CA and SA-25°CA cases at the instants analyzed in Fig. 8. However, possible lower heat losses at walls and a flawed prediction of flow and turbulence fields inside the bowl can globally affect the computed results. Therefore, different thermal diffusivity wall functions should be tested in the future, as well as 3D gas-exchange simulations are needed to improve the accuracy of the IVC fields initialization.

Similar observations and conclusions can be drawn for the two SI cases operated with a lean mixture (Fig. 7b) in terms of spark-timing effect.

Comparing Fig. 7a and Fig. 7b, the NH_3-air mixture dilution effect is assessed. As it can be inferred, at lean conditions (Fig. 7b) the spark time influence is predicted consistently with the experimental observation, while its effect on the further turbulent combustion speed inside the bowl is significantly lower if compared to measurements. This discrepancy is not detected at stoichiometric conditions (Fig. 7a), where the numerical-experimental agreement is stronger. Therefore, a global overestimation of the mixture dilution effect is provided by the numerical results. The main cause of this discrepancy could be attributed to a not accurate evolution of the flow and turbulence fields inside the piston bowl. Therefore, 3D simulations of the gas-exchange process are needed to clarify such aspects.

RFPI mode: results and discussion

The numerical analysis of the RFPI operation is carried out on the four measured operating conditions, reported in Table 3. As performed during the SI mode analysis, a comparison between computed results and experimental measurements in terms of in-cylinder pressure and apparent heat release rate (AHRR) trends is realized and included in Fig. 9.

Analyzing the stoichiometric conditions (Fig. 9a) and focusing on the initial ramp-up of the AHRR traces, the experimental effect produced by a variation of the injection duration (DOI) is properly captured. In fact, the selected numerical model allows to properly predict the differences observed in the auto-ignition process when the DOI is reduced from 550 µs to 450 µs, which yields to a weaker and slower premixed combustion development.

On the other hand, a slight numerical underestimation of the auto-ignition delay can be detected on both analyzed cases. This can be attributed to different causes. First, the accuracy of the numerical diesel injection profile, which should be improved to better replicate the experimental one. Second, the liquid spray is characterized by a possible too fast evaporation and mixing process, which requires the assessment of different break-up models. Third, the employed reaction kinetics mechanism, which perhaps does not properly predict the competition between C-reactions and N-reactions for the radical pool in presence of high NH_3 contents into reactants.

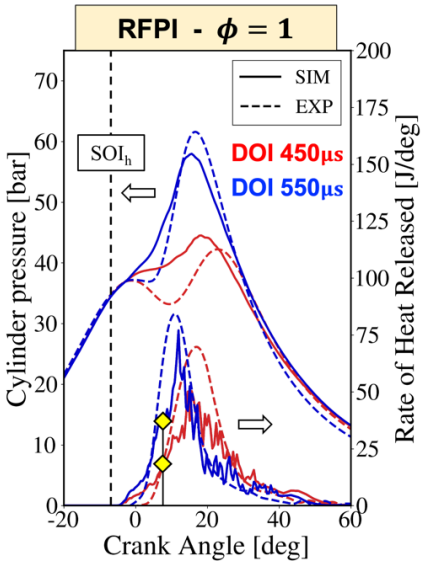

Fig. 9. RFPI mode: numerical-experimental comparison between pressure and apparent heat release rate (AHRR) evolutions inside the cylinder of the conditions in Table 3. The yellow squares spot the AHRR values of the instant analyzed in Fig. 10.

Advancing to the completion of the turbulent combustion stage inside the piston bowl (Fig. 9a, near the AHRR peak values), a general numerical underestimation of the energy released by the reactions is observed. In particular, the near-linear growth rate of the numerical AHRR during the fully turbulent stage (the 5-8 CAD interval for the DOI550 case, the 7-15 CAD interval for DOI450) is ≈ 45% lower than the experimental one, for both investigated conditions. This can be justified by an underestimation of the experimental turbulent flame speed. The TWM model approach, used in this work

to predict the RFPI combustion mode, does not include the flame-turbulence interaction effect, which for NH_3-air flames cannot be neglected. In fact, from optical measurements carried out in a constant-volume vessel at engine-like conditions, Lhuillier et al. [45] observed a turbulent-to-laminar velocity ratio which is almost doubled if NH_3 is used in place of CH_4. Therefore, the active flame front is underestimated, with a consequent weaker heat release rate. This statement is better clarified by Fig. 10, where a flame evolving inside the piston bowl is observed for both DOI durations at 8 °CA (highlighted with yellow squares in Fig. 9a), when the numerical-experimental discrepancies start to be significant in terms of AHRR evolution. During this stage, the flame is widening its active surface, hence the neglected flame-turbulence interaction by the TWM model gradually increases its impact on the numerical results.

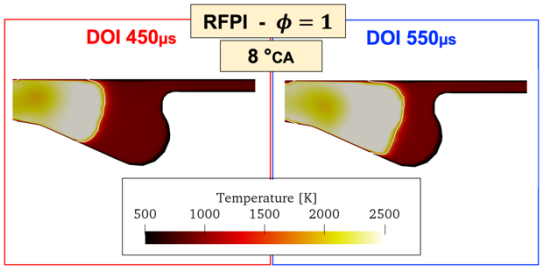

(a) **(b)**

Fig. 10. RFPI mode, ϕ = 1, 8 °CA: computed temperature distribution for conditions of Fig. 9a at the highlighted time instant with yellow squares (8 °CA). The white line detects the flame front position (normalized C = 0.5).

A quantitative estimation of the not-modelled flame-turbulence interaction, in terms of missing flame are increase, is not trivial. In fact, the flame front enhancement caused by this phenomenon depends on several magnitudes of the unburned mixture such as the turbulence intensity u', integral length scale L_t, laminar flame speed S_u and thickness δ_l (see Ξ_{eq} expression in Eq. 2). All these values are affected by the evolution in time of the flame front propagation, i.e. the higher the heat released by the flame front, the wider is the burnt gas volume, with the larger unburned mixture pressure and temperature. Therefore, this is an implicit problem, that can be solved only through 3D-CFD numerical simulations with an improved TWM model version. A preliminary proposal to embed the flame-turbulence interaction phenomenon inside the TWM model is described in the next paragraph.

Concerning the last two RFPI cases, operated instead with a leaner NH_3-air premixed mixture (Fig. 9b), similar observations and conclusions to stoichiometric cases can be drawn.

The NH_3-air mixture dilution effect can be finally analyzed by comparing Fig. 9a and Fig. 9b. Observing the initial ramp-up of the AHRR traces, the experimental findings clearly exhibit a reduction of the auto-ignition delay of the diesel-ammonia-air mixture when the NH_3 content is reduced. This advances the next premixed flame propagation, with higher in-cylinder peak pressures detected for both DOI values. The numerical model seems able to replicate such increased mixture reactivity in presence of a reduction of the ammonia energy fraction. In fact, both computed DOI cases are characterized by an increase of the in-cylinder peak pressure when the ϕ is reduced. Nevertheless, the slight numerical underestimation of the auto-ignition delay, previously observed under a DOI-only variation, here impacts on the quantitative numerical-experimental agreement. This results in a global underestimation of the ϕ impact, if compared to measurements.

Improved TWM model: a preliminary proposal

According to the results discussed for the RFPI mode, the employed version of TWM model exhibits limitations in predicting the experimental reaction rate during the fully turbulent combustion stage. The most convincing explanation is the not modelled enhancement of the flame front area caused by the turbulence stretch effect.

A possible solution to this shortage is to include the FAE model approach (Eqs. 1 and 2), employed for the SI combustion, inside the TWM framework. Both equations are solved from the occurrence of the auto-ignition event. The heat released from the diesel-NH_3 combustion is introduced into Eq. 1 through the source term $\dot{\omega}_{ign}$, which can be modelled as,

$$\dot{\omega}_{ign} = -\rho_u \dot{c} \quad (6)$$

Here, $\dot{c}$ is the time variation of the normalized C field, which can be defined as,

$$c = \frac{C - C_{min}}{C_{max} - C_{min}} \quad (7)$$

being C_{min} and C_{max} the progress variable values in the unburned and burned mixture, respectively.

The laminar-to-turbulent flame transition is still modelled through the f parameter of Eq. 2. When this evolution is completed (f = 1), the NH_3-air premixed flame can be considered to be no more affected by the ignition process driven by the diesel pilot injection. Therefore, Eqs. 3, 4 and 5 can be disabled and the turbulent premixed combustion

evolution is fully handled by Eqs. 1 and 2, similarly to the approach used for the SI mode.

Conclusions

In this study, consolidated 3D-CFD approaches are used to model the premixed NH_3-air combustion in both spark-ignition (SI) and reactive-fuel pilot-ignition (RFPI) modes. The flame area model (FAM) is selected to predict SI operation, while the tabulated well-mixed (TWM) model for RFPI cases. A flat-head metal engine is chosen as experimental reference, where different NH_3-air equivalence ratios and ignition timings are measured under constant engine speed. The objective of this work, which is the first step of a large-scale study, is to identify the most critical aspects related to the NH_3 combustion modelling in ICEs, pointing out the main challenges that urged to be addressed by the academical/industrial community.

In SI mode, the employed numerical approach can predict the measured effect of a spark-timing variation, also in presence of an ammonia dilution. However, the following aspects require further improvements,

a) Underestimation of the measured laminar-turbulent transition stage duration.

b) Weaker heat release rate from in-bowl combustion when the spark-timing is advanced.

c) Overestimation of the heat release rate from in-crevices combustion when the spark-timing is advanced.

If the first effect is probably caused by a not modelled electrical delay, the other two issues can be related to multiple aspects, like 1) a higher ammonia quantity is forced into the squish region; 2) a limited flame area extension is observed when the ignition time is advanced, because of the narrow piston-head distance; 3) lower heat losses at the walls; 4) an inaccurate prediction of flow and turbulence fields inside the bowl (swirl motion is initialized at IVC). Therefore, to clarify such aspects, 3D simulations of the gas-exchange process are needed, as well as different thermal diffusivity wall functions should be tested.

In RFPI mode, the applied numerical method demonstrated to capture the measured effect of a variation of the diesel injection duration, also when the ammonia content is reduced. However, challenges are represented by the numerical underestimation of,

a) the auto-ignition delay of the diesel-NH_3-air mixture, and

b) the turbulent flame speed observed from experimental findings.

The first aspect can be caused by 1) low accuracy of the numerical diesel injection profile; 2) too fast evaporation and mixing process of the liquid diesel spray; 3) advancements required by the selected reaction mechanism. The second issue is probably related to the lack of the flame-turbulence interaction modeling, which can be solved by including flamelet-based approaches in the TWM model. To solve this last deficiency, a preliminary improvement of the TWM model has been proposed and it will be tested in a future work.

Conflicts of Interest

The authors declare no conflict of interest. The funders had no role in the design of the study; in the collection, analyses, or interpretation of data; in the writing of the manuscript, or in the decision to publish the results.

References

1. Wilkinson I. Siemens green Ammonia. 1st NH3 European event. Netherlands: Rotterdam; 2017.
2. Valera-Medina A, Xiao C, Owen-Jones M, David WIF, Bowen PJ. Ammonia for power. Prog Energy Combust Sci. 2018; 69, 63-102; doi: https://doi.org/10.1016/j.pecs.2018.07.001.
3. Lhuillier C, Brequigny P, Contino F, Rousselle C. Combustion Characteristics of Ammonia in a Modern Spark-Ignition Engine. SAE Tech Paper. 2019; 2019-24-0237; doi: https://doi.org/10.4271/2019-24-0237.
4. Jespersen MC, Rasmussen TØH, Ivarsson A. Widening the operation limits of a SI engine running on neat ammonia. Fuel. 2024; 358, 130159; doi: https://doi.org/10.1016/j.fuel.2023.130159.
5. Uddeen K, Tang Q, Shi H, Magnotti G, Turner J. A novel multiple spark ignition strategy to achieve pure ammonia combustion in an optical spark-ignition engine. Fuel. 2023; 349, 128741; doi: https://doi.org/10.1016/j.fuel.2023.128741.
6. Mounaïm-Rousselle C, Mercier A, Brequigny P, Dumand C, Bouriot J, Houillé S. Performance of ammonia fuel in a spark assisted compression Ignition engine. Int J Engine Research. 2022; 23(5), 781-792; doi: https://doi.org/10.1177/14680874211038726.
7. Reggeti S, Kane S, Northrop W. Experimental Investigation of Spark-Assisted Compression-Ignition with Ammonia-Hydrogen Blends. J Ammonia Energy. 2023; 1(1); doi: https://doi.org/10.18573/jae.21.
8. Lhuillier C, Brequigny P, Contino F, Rousselle C. Performance and Emissions of an Ammonia-Fueled SI Engine with Hydrogen Enrichment. SAE Tech Paper. 2019; 2019-24-0137; doi: https://doi.org/10.4271/2019-24-0137.
9. Mounaïm-Rousselle C, Brequigny P, Dumand, C, Houillé, S. Operating limits for ammonia fuel spark-

ignition engine. Energies. 2021; 14 (14), 4141; doi: https://doi.org/10.3390/en14144141.
10. Frigo S, Gentili R. Analysis of the behaviour of a 4-stroke Si engine fuelled with ammonia and hydrogen. Int J Hydro Energy. 2013; 38 (3), 1607–1615; doi: https://doi.org/10.1016/j.ijhydene.2012.10.114.
11. Koike M, Suzuoki T, Takeuchi T, Homma T, Hariu S, Takeuchi Y. Cold-start performance of an ammonia-fueled spark ignition engine with an on-board fuel reformer. Int J Hydro Energy. 2021; 46 (50), 25689–25698; doi: https://doi.org/10.1016/j.ijhydene.2021.05.052.
12. Kane SP, Northrop WF. Thermochemical recuperation to enable efficient ammonia-diesel dual-fuel combustion in a compression ignition engine. Energies. 2021; 14 (22), 7540; doi: https://doi.org/10.3390/en14227540.
13. Dimitriou P, Javaid R. A review of ammonia as a compression ignition engine fuel. Int J Hydro Energy. 2020; 45(11), 7098-7118; doi: https://doi.org/10.1016/j.ijhydene.2019.12.209.
14. Dupuy A, Brequigny P, Schmid A, Frapolli N, Mounaïm-Rousselle C. Experimental study of RCCI engine – Ammonia combustion with diesel pilot injection. J Ammonia Energy. 2023; 1(1); doi: https://doi.org/10.18573/jae.6.
15. Hiraoka K, Matsunaga D, Kamino T, Honda Y, Toshinaga K, Murakami Y, Nakamura H. Experimental and numerical analysis on combustion characteristics of ammonia and diesel dual fuel engine. SAE Tech Paper. 2023; 2023-32-0102; doi: https://doi.org/10.4271/2023-32-0102.
16. Imamori Y, Takahashi T, Ueda H, Yamada S, Tanaka T, Kogure R. Experimental and Numerical Investigations of Emission Characteristics from Diesel-Ammonia-Fueled Industry Engines. SAE Tech Paper. 2023; 2023-32-0064; doi: https://doi.org/10.4271/2023-32-0064.
17. Liu J, Wang X, Zhao W, Sun P, Ji Q. Effects of ammonia energy fraction and diesel injection parameters on combustion stability and GHG emissions characteristics in a low-loaded ammonia/diesel dual-fuel engine. Fuel. 2024; 360, 130544; doi: https://doi.org/10.1016/j.fuel.2023.130544.
18. Rousselle C, Brequigny P, Dupuy A. Impact of Splitting n-Dodecane Pilot Injection on Ammonia RCCI Engine. SAE Tech Paper. 2023; 2023-24-0076; doi: https://doi.org/10.4271/2023-24-0076.
19. Mi S, Wu H, Pei X, Liu C, Zheng L, Zhao W, Qian Y, Lu X. Potential of ammonia energy fraction and diesel pilot-injection strategy on improving combustion and emission performance in an ammonia-diesel dual fuel engine. Fuel. 2023; 343, 127889; doi: https://doi.org/10.1016/j.fuel.2023.127889.
20. Zhang R, Chen L, Wei H, Li J, Ding Y, Chen R; Pan J. Experimental investigation on reactivity-controlled compression ignition (RCCI) combustion characteristic of n-heptane/ammonia based on an optical engine. Int J Engine Research. 2023; 24(6), 2478-2488; doi: https://doi.org/10.1177/14680874221124452.
21. Sforza L, Abdelwahid S, Lucchini T, Onorati A. Ultra-Lean Premixed Turbulent Combustion: Challenges of RANS Modelling. Energies. 2022; 15, 5947; doi: https://doi.org/10.3390/en15165947.
22. Sforza L, Lucchini T, D'Errico G. 3D-CFD Methodologies for a Fast and Reliable Design of Ultra-Lean SI Engines. SAE Tech Paper. 2022; 2022-37-0006; doi: https://doi.org/10.4271/2022-37-0006.
23. Lucchini T, D'Errico G, Cerri T, Onorati A, Hardy G. Experimental Validation of Combustion Models for Diesel Engines Based on Tabulated Kinetics in a Wide Range of Operating Conditions. SAE Tech Paper. 2017; 2017-24-0029; doi: https://doi.org/10.4271/2017-24-0029.
24. Schirru A, Lucchini T, D'Errico G, Mehl M, Hilfiker T, Soltic P. Numerical investigation on the use of Dimethyl Ether (DME) as an alternative fuel for compression-ignition engines. Fuel. 2023; 354, 129434; doi: https://doi.org/10.1016/j.fuel.2023.129434.
25. Gianetti G, Sforza L, Lucchini T, D'Errico G, Soltic P, Rojewski J, Hardy G. CFD modeling of combustion of a natural gas Light-Duty Engine. Energy Proc. 2018; 148, 954 – 961; doi: https://doi.org/10.1016/j.egypro.2018.08.067.
26. Sforza L, Lucchini T, D'Errico G, Gianetti G, Beatrice C, Tunestål P. A Numerical Methodology for the Design of Active Prechambers in Spark-Ignition Engines. Combust Sci Tech. 2023; doi: https://doi.org/10.1080/00102202.2023.2219450.
27. Ramognino F, Sforza L, Lucchini T, D'Errico G, Onorati A. A methodology to initialize tumble flow fields for fast 3D-CFD simulations of pent-roof SI engines. J Phys: Conference Series. 2022; 2385, 012066; doi: https://doi.org/10.1088/1742-6596/2385/1/012066.
28. Lucchini T, D'Errico G, Paredi D, Sforza L, Onorati A. CFD Modeling of Gas Exchange, Fuel-Air Mixing and Combustion in Gasoline Direct-Injection Engines. SAE Tech Paper. 2019; 2019-24-0095; doi: https://doi.org/10.4271/2019-24-0095.
29. Sforza L, Lucchini T, Gianetti G, D'Errico G. Development and Validation of SI Combustion Models for Natural-Gas Heavy-Duty Engines. SAE Tech Paper. 2019; 2019-24-0096; doi: https://doi.org/10.4271/2019-24-0096.
30. Ramognino F, Sforza L, Cerri T, Lucchini T, Onorati A, Novella R. A fast and reliable CFD approach to design hydrogen SI engines for

industrial applications. SAE Tech Paper. 2023; 2023-01-1208; doi: https://doi.org/10.4271/2023-01-1208.
31. Ramognino F, Sforza L, D'Errico G, Gomez-Soriano J, Onorati A, Novella R. CFD Modelling of Hydrogen-Fueled SI Engines for Light-Duty Applications. SAE Tech Paper. 2023; 2023-24-0017; doi: https://doi.org/10.4271/2023-24-0017.
32. Weller HG, Tabor G, Gosman AD, Fureby C. Application of a Flame-Wrinkling LES Combustion Model to a Turbulent Mixing Layer. Symp (Int) Combust. 1998; 27(1), 899–907; doi: https://doi.org/10.1016/S0082-0784(98)80487-6.
33. Herweg R, Maly R. A Fundamental Model for Flame Kernel Formation in S. I. Engines. SAE Tech Paper. 1992; 922243; doi: https://doi.org/10.4271/922243.
34. Peters, N. Turbulent Combustion; Publisher: Cambridge University Press, 2000. https://doi.org/10.1017/CBO9780511612701
35. Cuoci A, Frassoldati A, Faravelli T, Ranzi E. OpenSMOKE++: An object-oriented framework for the numerical modeling of reactive systems with detailed kinetic mechanisms. Comp Phys Comm. 2015; 192, 237-264, doi: https://doi.org/10.1016/j.cpc.2015.02.014.
36. Stagni A, Arunthanayothin S, Dehue M, Herbinet O, Battin-Leclerc F, Bréquigny P, Mounaïm-Rousselle C, Faravelli T. Low- and intermediate-temperature ammonia/hydrogen oxidation in a flow reactor: Experiments and a wide-range kinetic modeling. Chem Engin J. 2023; 471, 144577; doi: https://doi.org/10.1016/j.cej.2023.144577.
37. Lucchini T, D'Errico G, Onorati A, Frassoldati, A, Stagni A, Hardy G. Modeling Non-Premixed Combustion Using Tabulated Kinetics and Different Fame Structure Assumptions. SAE Int J Engines. 2017; 10(2), 593–607; doi: https://doi.org/10.4271/2017-01-0556
38. Lehtiniemi H, Zhang Y, Rawat R, Mauss F. Efficient 3-D CFD Combustion Modeling with Transient Flamelet Models. SAE Tech Paper. 2008; 2008-01-0957; doi: https://doi.org/10.4271/2008-01-0957.
39. Ranzi E, Frassoldati A, Stagni A, Pelucchi M, Cuoci A, Faravelli T. Reduced kinetic schemes of complex reaction systems: Fossil and biomass-derived transportation fuels. Int J Chem Kinetics. 2014; 46 (9), 512-542; doi: https://doi.org/10.1002/kin.20867.
40. C1-C16 HT mechanism (Version 2003, March 2020). Available online: https://creckmodeling.chem.polimi.it/menu-kinetics/menu-kinetics-detailed-mechanisms/107-category-kinetic-mechanisms/402-mechanisms-1911-tot-ht/ (accessed on 05 May 2023).
41. Lucchini T, Della Torre A, D'Errico G, Montenegro G, Fiocco M, Maghbouli A. Automatic Mesh Generation for CFD Simulations of Direct-Injection Engines. SAE Tech Paper. 2015; 2015-01-0376; doi: https://doi.org/10.4271/2015-01-0376.
42. Sforza L, Lucchini T, Montenegro G, Aksu C, Shiraishi T. Modeling the Effects of the Ignition System on the CCV of Ultra-Lean SI Engines using a CFD RANS Approach. SAE Tech Paper. 2021; 2021-01-1147; doi: https://doi.org/10.4271/2021-01-1147.
43. Gianetti GG, Lucchini T, Sforza L, Onorati A, Lombardi C, Cavagnero C. Numerical and Experimental Investigation on Passive Prechamber Configurations Able to Operate at Low Engine Speed and Load. SAE Tech Paper. 2023; 2023-24-0031; doi: https://doi.org/10.4271/2023-24-0031.
44. Ramognino F, Sforza L, Lucchini T, Welch C, Böhm B, Onorati A. A CFD ignition model to predict average-cycle combustion in SI engines with extreme EGR levels. Int J Engine Research. 2023; doi: https://doi.org/10.1177/14680874231214575.
45. Lhuillier C, Brequigny P, Contino F, Mounaïm-Rousselle C. Experimental investigation on ammonia combustion behavior in a spark-ignition engine by means of laminar and turbulent expanding flames. Proc Combust Inst. 2021; 38, 5859-5868; doi: https://doi.org/10.1016/j.proci.2020.08.058.